A Buckingham interatomic potential for thallium oxide (Tl 2 O): Application to the case of thallium tellurite glasses

Raghvender Raghvender, Assil Bouzid, David Hamani, Philippe Thomas, Olivier Masson

ScienceDirect
www.sciencedirect.com

Computational Materials Science 00 (2021) 1–8

Journal Logo

A Buckingham interatomic potential for thallium oxide (Tl_2O): application to the case of thallium tellurite glasses.

Raghvender*, Assil Bouzid, David Hamani, Philippe Thomas, Olivier Masson

Institut de Recherche sur les Céramiques (IRCER), CNRS UMR 7315, Université de Limoges, Centre Européen de la Céramique, 12 rue Atlantis, 87068 Limoges, France

Abstract

An interatomic potential for simulating the structural properties of thallium (I) oxide (with oxidation state +1) based compounds has been developed by fitting to the experimental crystalline structures of α-$Tl_2Te_2O_5$, $Tl_2Te_3O_7$ and Tl_2TeO_3 simultaneously. The obtained potentials are subsequently verified and validated by optimizing additional Tl(I)−O based compounds, leading to a good agreement of the lattice constants with experimental data. Amorphous $(TlO_{0.5})_x-(TeO_2)_{1-x}$ systems where then produced by classical molecular dynamics and their structural properties compared to experimental measurements.

Keywords: Thallium (I), Buckingham interatomic potential, shell model, oxide glass.

1. Introduction

TeO_2-based materials exist in crystalline and amorphous forms, featuring high dielectric constant [1], high refractive index [2], good infrared transmissivity, good optical properties [10], strong thermal and chemical stability [11, 12], low glass transition temperatures and high third-order optical non-linearity ($\chi^{(3)}$ = 1.9572 x 10^{-20} m^2/V^2) [13] with several orders of magnitude larger than that of conventional silicate and borate glasses [14]. These properties make TeO_2-based glasses substantially promising for applications in areas such as laser light modulators [2], pressure sensors and optical switching devices [15]. Despite the large efforts undertaken to study these materials, the link between the macroscopic measurable properties and the intimate features of the atomic-scale structure remain elusive.

In practice, pure TeO_2 is a conditional glass former [16] and requires a fast quenching rates to achieve stable amorphous samples [17, 18, 19, 20, 21, 22]. This limitation could be overcome by mixing TeO_2 with other modifier oxides (MO) [2, 23] such as Li_2O, Na_2O, K_2O, ZnO [24]. In particular, thallium oxide (Tl_2O) has attracted a great attention as a MO, as its addition, contrary to other MO leads to maintain the amplitude of the high optical non-linearity of the TeO_2-based materials [25, 26] despite the structural depolymerization of the glasses evidenced by Raman spectroscopy [27, 28, 29]. Thallium is a rare element of the boron group that exists in two oxide forms: thallous oxide (Tl_2^+O) and thallic oxide ($Tl_2^{3+}O_3$). While Tl_2^+O has been widely used as a MO in TeO_2-based glass [25, 28, 23, 26], we are not aware of any work that demonstrates the efficiency of $Tl_2^{3+}O_3$ as a MO. As such, we here focus solely on developing an empirical model for the investigation of Tl_2^+O MO in TeO_2-based materials.

The atomic scale structure of TeO_2 glass is essentially made of distorted TeO_4 disphenoid [27, 22] with an electronic lone pair (LP) laying in the vicinity of the Te atom. These structural units are linked to each other through Te−O−Te linkages. Incorporation of a modifier oxide into TeO_2 amorphous phase leads to a reduction in coordination number of Te^{4+} cation by the transformation of initially present TeO_4 disphenoids into TeO_3 trigonal pyramidal units [2]. While this decrease in coordination number generally leads to a decrease of the non-linear optical response of the material, the opposite trend is observed in the case of Tl_2O modifier. Beside these general trends in the structural evolution of Tl_2O modified TeO_2 glasses, the Tl^+ local environments in the amorphous matrix remains to a large extent unknown. At the experimental side, beside studies based on Raman spectroscopy [27], experimental results on $(M_2O)_x-(TeO_2)_{1-x}$ (M: alkali modifier ion; x: concentration) glasses focused more on the macroscopic properties rather than the atomic-scale description of the glass. At the theoretical

*Author in correspondence.
Email addresses: raghvender.raghvender@unilim.fr (Raghvender), assil.bouzid@unilim.fr (Assil Bouzid)

side, no study of the Tl_2O-TeO_2 systems exist, to the best of our knowledge.

At this level, modelling can help one to disentangle the role of thallium oxide in structural and optical properties of Tl_2O-TeO_2 binary glasses. Atomistic models can be obtained through first-principles molecular dynamics based on a quantum mechanical description of the particles interaction. Nevertheless, such a technique is computationally expensive which limits its application to either small systems or short time-scales. Alternatively, classical molecular dynamics based on empirical interatomic potentials (IAPs) offer the possibility of modelling large glassy systems over long periods of time at a very reasonable computational cost and keeping a good accuracy.

Modelling Tl_2O-TeO_2 glasses requires the development of an IAP that accounts for elemental interactions in this system. To date, only one classical IAP exists for $Te^{4+}-O^{2-}$ interaction. This potential has been developed by Gulenko *et al.* [30] and further improved by Torzuoli *et al.* [31]. In these studies, the authors adopted a fully ionic description (i.e. electronic charges equal to oxidation number) of the system with a Buckingham core-shell potential formulation that leads to very good results on reproducing lattice parameters of various TeO_2 crystalline phases within 2% of mean absolute error. In addition, their potential was used to model glassy TeO_2 leading to structural properties in fair agreement with experimental measurements.

In the present work, we focus on developing a classical IAP for Tl^+-O^{2-} interaction in order to model amorphous $(TlO_{0.5})_x-(TeO_2)_{1-x}$ compounds (for convenience, we use hereafter $TlO_{0.5}$ notation instead of Tl_2O). Our potential is tested against various Tl(I) containing oxides and proved to be transferable. Furthermore, we produce amorphous models of various $(TlO_{0.5})_x-(TeO_2)_{1-x}$ glasses featuring a good agreement with experimental measurements.

This paper is organized as follows. Following the introduction, section 2 describes the computational approach and fitting criteria used to develop the classical Tl^+-O^{2-} IAP. Section 3 is devoted to the IAP transferability tests on various Tl (I) based compounds and its validity on the amorphous description of $(TlO_{0.5})_x-(TeO_2)_{1-x}$ systems. Finally, concluding remarks are presented in the section 4.

2. Methodology

2.1. Theory

In this work, we adopt the Buckingham formulation of the classical IAP [32] in conjunction with an electrostatic interaction model that turned successful on modelling a variety of materials [30],[33]. In practice, the potential energy U_{ij} of a given system is written as follows:

$$U_{ij} = A_{ij}e^{-r/\rho_{ij}} - C_{ij}r^{-6} + \frac{q_i q_j}{4\pi\varepsilon_0}\frac{1}{r}, \quad (1)$$

where A_{ij}, ρ_{ij} and C_{ij} are the Buckingham potential parameters and q_i is the charge (=oxidation number) of ion i. The first term in Eq. (1) describes the electronic repulsion at the short range due to the overlap of closed electron shells. The middle term in Eq. (1) represents the attractive London dispersion contribution. Finally, the last term contributing to U_{ij} is the coulombic interaction. Due to the long range nature of this term, it requires a special treatment during its calculation which is handled through the Ewald summation technique [34].

Classical description of ions that carry an electronic LP, such as Te^{4+} and Tl^+, requires a careful account of their ionic polarizabilities. We resort to the Dick and Overhauser's shell model [35] that allows for an analytical description of the ionic polarisibility. In this technique, a mass-less shell is attached to the massive core of the ion. The core and the shell of the same ion are coloumbically screened, but coupled through a harmonic spring of force constant K_h and possibly an anharmonic force constant K_{ah}. This scheme induces a polarization on the considered ion as its associated shell is displaced. The potential energy contribution of this core-shell model, E_{cs} is given by:

$$E_{cs} = \frac{1}{2!}K_h r_{cs}^2 + \frac{1}{4!}K_{ah} r_{cs}^4, \quad (2)$$

where r_{cs} is the distance between ionic core and its associated shell. This model allows one to derive environment based polarizabilities, α, which are expressed as:

$$\alpha = \frac{q_{sh}^2}{K_h}, \quad (3)$$

where q_{sh} is the charge assigned to the shell of the ion.

Coupling the Buckingham interaction potential with the core-shell model allows one to develop classical IAPs by relying on a proper account of the ionic polarizibility of the system, as implemented in the General Utility Lattice Program (GULP) [36] software.

2.2. Deriving interatomic potential for Tl^+-O^{2-}

In order to produce and study the amorphous structure of thallium tellurite glasses, IAPs accounting for Te, Tl, and O interactions are required. In previous works, Gulenko *et al.* [30] and Torzuoli *et al.* [31] have proposed a Buckingham potential model for Te^{4+} and O^{2-} that allows a good description of TeO_2-based crystals and pure TeO_2 glass. In this work, we intend to extend this model to be able to describe Te−Tl−O compounds. In practice, energy parameters (see Eq. 1) accounting for the Tl^+-O^{2-} and Tl^+-Tl^+ interactions need to be fitted on the basis of experimental data.

We note that core-shell interactions used by Gulenko *et al* [30] are somehow unconventional. In particular, instead of a direct Te shell and O shell interaction, the authors allowed Te core to interact directly with O shell. Following the same legacy, in this work we allow O shell to interact with Tl core instead of Tl shell, as illustrated in Fig. 1.

In order to optimize the potential parameters, we consider three Te−Tl−O crystal structures, namely α-$Tl_2Te_2O_5$ [37], $Tl_2Te_3O_7$ [38] and Tl_2TeO_3 [39] (see crystal structure projections along c axis in Fig. 2) simultaneously to fit the Tl^+-O^{2-}

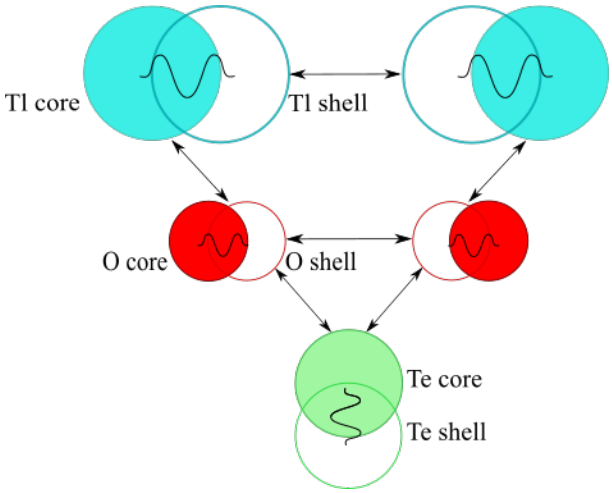

Figure 1. Schematic representation of interactions between shells and/or cores in Te−Tl−O systems used in our work.

and $Tl^{+}-Tl^{+}$ interaction model. In particular, we consider experimental lattice parameters and atomic positions as observables to be reproduced by the Buckingham interaction model.

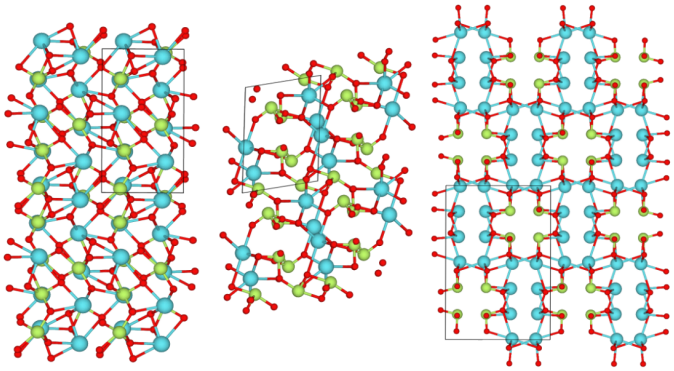

(a). α-$Tl_2Te_2O_5$ (b). $Tl_2Te_3O_7$ (c). Tl_2TeO_3

Figure 2. Three crystalline thallium tellurite crystal structures used in the fit of IAP. (a) α-$Tl_2Te_2O_5$: space group - $P2_1/n$, (b) $Tl_2Te_3O_7$: space group - P_1, (c) Tl_2TeO_3 : space group - Pban. Color code: oxygen (red), tellurium (green) and thallium (cyan).

The convergence of a fit is evaluated by computing the final sum of squares between these experimental observables and their calculated counterpart obtained through the IAP model. The sum of squares, F, is defined as follows:

$$F = \sum_{\text{observables}} w * (f_{calc} - f_{obs})^2, \quad (4)$$

where f_{calc} and f_{obs} are the calculated and observed quantities and w is a weighting factor. F is minimized with respect to the variable potential parameters using the Newton-Raphson method. In addition, in the case where more than one set of parameters led to F convergence, the one that leads to the least deviation from the experimental lattice parameters is selected.

In our strategy, we start by adding a $Tl^{+}-O^{2-}$ energy term to the $Te^{4+}-O^{2-}$ Buckingham potential from Ref. [40]. The initial parameters of this potential energy term were initialized

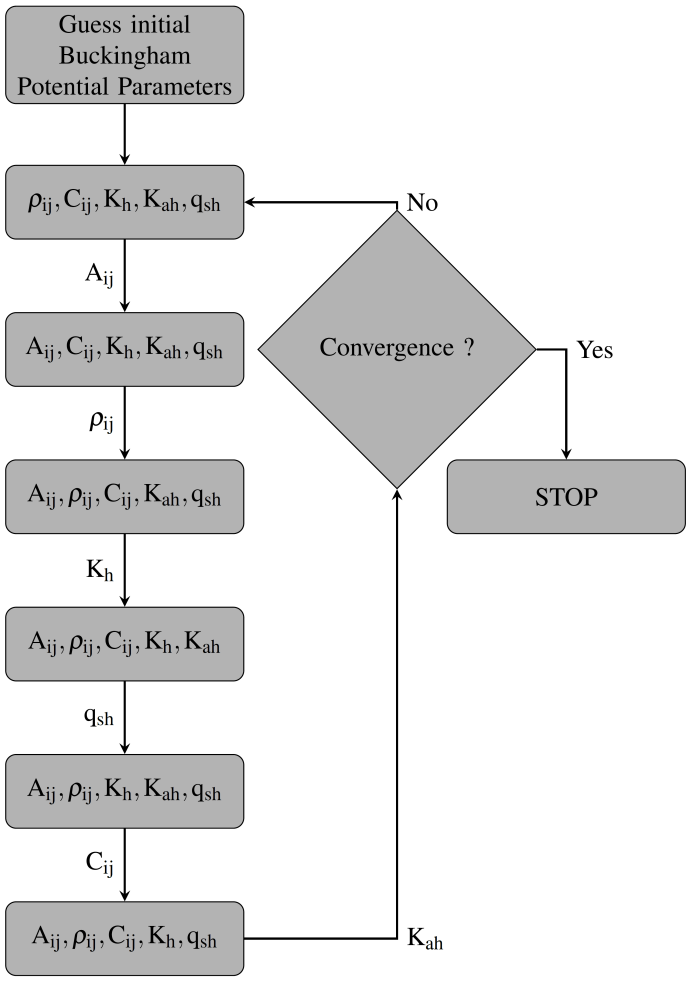

Figure 3. Illustration of the fitting flowchart used to develop the Te−Tl−O IAP. Parameters fixed during the fit are shown in rectangular boxes, while the variable parameter is displayed along the arrows.

to $Tl^{3+}-O^{2-}$ parameters available in Woodley library of potentials for GULP [41]. Then, we fix ρ_{ij}, C_{ij}, q_{sh}, K_h and K_{ah} and vary A_{ij} from 100 eV to 5000 eV. The value of A_{ij} yielding the best fit has then been kept fixed and other parameters were subsequently varied. Following the flowchart presented in Fig. 3, ρ_{ij} is varied in the interval 0.1 to 0.6 Å, K_h from 10 to 200 eV.$Å^{-2}$, q_{sh} from 0.2 to 0.6 e, C_{ij} from 0 to 50 eV.$Å^{-6}$ and lastly, K_{ah} from 0 to 200 eV.$Å^{-4}$.

After this loop of fitting is finished, the obtained $Tl^{+}-O^{2-}$ interaction parameters are then fixed and a new interaction term is added to account for the $Tl^{+}-Tl^{+}$ interaction. We found that adding such an interaction term is required in order to prevent the systems from undergoing important geometrical deformation. The initial ρ_{ij} and C_{ij} values are fixed to those obtained in the case of $Tl^{+}-O^{2-}$ interaction and A_{ij} is varied to minimise the final sum of squares. As in the case of $Tl^{+}-O^{2-}$ interaction, a complete loop on the potential parameters is performed following the fit flowchart (Fig. 3) until convergence is achieved.

After these two loops of optimization we obtained a reasonable parametrization of the $Tl^{+}-O^{2-}$ and $Tl^{+}-Tl^{+}$ potentials. In order to achieve a full convergence of the Buckingham interatomic potential for Te−Tl−O compounds and ensure its stability, we repeatedly carried out the potential parameters fitting until their values reach convergence and do not change significantly when refitted. The final Buckingham potential parameters for Te−Tl−O compounds are listed in table 1.

Buckingham Potential

	A (eV)	ρ (Å)	C (eV.Å^{-6})
	Torzuoli *et al.* [31]		
Te_c^{4+}-O_{sh}^{2-}	1631.810731	0.346336	0.020139
O_{sh}^{2-}-O_{sh}^{2-}	47902.536233	0.175930	33.029759
	This Work		
Tl_c^{+}-O_{sh}^{2-}	826.731161	0.341763	17.097819
Tl_{sh}^{+}-Tl_{sh}^{+}	924.000025	0.392193	9.906808

Shell Model

	K_h (eV.Å^{-2})	K_{ah} (eV.Å^{-4})	q_{sh}(e)
	Torzuoli *et al.* [31]		
Te^{4+}	30.827429	90.0	-1.975415
O^{2-}	61.600546	0.00	-3.122581
	This Work		
Tl^{+}	111.754795	81.0	-2.852493

Table 1. Obtained Buckingham IAP parameters for thallium core-oxygen shell and thallium shell-thallium shell interaction along with the charges and spring constants. Data for Te_c^{4+}-O_{sh}^{2-} and O_{sh}^{2-}-O_{sh}^{2-} interactions have been taken from Torzuoli *et al.* [31] work.

3. Results and discussion

3.1. Validation of the interatomic potential

The quality of an IAP is inherently related to its capability of describing various chemical environments. As such, we test the transferrability of the obtained IAP by considering several thallium (I) oxide based crystalline compounds. The considered crystals were extracted from the Open Quantum Materials Database [42], [43] and listed in table 2. Other than the IAPs derived in this work, the potential parameters for atomic interaction in compounds mentioned in table 2 were taken from "Database of Published Interatomic Potential Parameters - UCL" [53]. The sources of all the considered potentials are cited in table 2. For each compound, a variable cell geometry optimization is achieved through the BFGS algorithm [44, 45, 46, 47]. Final results are presented in table 2.

The obtained mean absolute errors (MAE) on the lattice parameters of various Tl (I) based compounds show a very good accuracy with values less than 6% (see Tab. 2). Such a good result proves the versatility of our potential in accounting for different Tl(I) environments ranging from TlO_3 to TlO_9 units. Nevertheless, one remarks that simple Tl_2O shows relatively high MAE that reflects the large elongation of the cell along the c direction. This result is most likely ascribed to the layered arrangement of crystalline Tl_2O compound that would require a higher level of theory to be properly described [48].

ICSD No.	Tl^{+} based compound	Tl^{+} environment	a (%)	b (%)	c (%)	MAE (%)
50457	$TlCuPO_4$ [4, 5]	TlO_3	-8.56	0.97	-1.93	3.82
33579	$TlGaO_2$ [6]	TlO_9	6.62	6.62	-0.46	4.57
202028	Na_3TlO_2 [7]	TlO_3	4.93	1.92	-7.92	4.92
98627	$Tl_2Ni_4P_4O_{15}$ [8, 5]	TlO_3/TlO_5	0.04	0.81	0.82	0.56
74811	$TlZnPO_4$ [9, 5]	TlO_4/TlO_5	-2.63	1.26	12.70	5.53
98625	$TlNi_4P_3O_{12}$ [8, 5]	TlO_6	0.63	-4.92	0.73	2.09
98626	$Tl_4NiP_6O_{24}$ [8, 5]	TlO_4/TlO_6/TlO_7	0.40	2.04	1.93	1.46
77699	Tl_2O	TlO_3	8.89	2.78	18.83	10.17
86782	α-$Tl_2Te_2O_5$ [31]	TlO_4	2.56	-4.95	2.11	3.21
200965	Tl_2TeO_3 [31]	TlO_4	0.15	-5.69	8.76	4.87
150779	$Tl_2Te_3O_7$ [31]	TlO_3/TlO_4	-0.68	-0.30	1.15	0.71

Table 2. Percentage change in reproducing lattice parameters (a, b, c) compared with experiments and the mean absolute error (MAE) of investigated crystalline Tl (I) based oxides has been shown. A cut-off bond length of 3 Å is used in describing different Tl (I) environments (for the case of $TlGaO_2$, cut-off of 3.3Å is used).

For this reason, and after few tests, we ruled out pure Tl_2O from the potential fitting procedure and only considered crystalline phases of α-$Tl_2Te_2O_5$, $Tl_2Te_3O_7$ and Tl_2TeO_3. For these three compounds, a very good accuracy in predicting experimental lattice parameters is obtained. Furthermore, we present in table 3 the experimental and calculated $Tl^{+}-O^{2-}$ bond distances in the α-$Tl_2Te_2O_5$, $Tl_2Te_3O_7$ and Tl_2TeO_3 crystalline systems and find that they are well reproduced compared to experiments with an average error of 1.8%.

3.2. Classical molecular dynamics (MD) study of thallium tellurite glasses

We further validate our potential in the case of thallium tellurite glasses and show its capability in producing good description of their glassy states. We here stick to a general validation of the IAP and do not discuss the atomic scale structures of these glasses as this requires the production of extended atomistic models which goes beyond the scope of this work. In practice, we generate random initial configurations for $(TlO_{0.5})_x - (TeO_2)_{1-x}$ with concentrations x = 0.1, 0.2, 0.3, 0.4, and 0.5, using Packmol software [49]. The detailed simulation cell information can be found in table 4.

We carried out MD simulations as implemented in the DL_POLY software package [50] using our IAP presented in table 1. An integration time step of 1.0 fs is used to integrate the Newton's equations of motion. Starting from the random configurations, each configuration underwent a thermal cycle featuring 50ps at 2000K, 70ps at 1500K, 70ps at 1000K, 70ps at 600K and lastly maintained for 70ps at 300K (see Fig. 4(a)). These runs are performed at fixed density in the NVT (constant number of particles, volume and temperature) ensemble. We ensured that at high temperature all the configurations exhibited a considerable diffusion and completely lost memory of the initial state. As maintaining the system at the

Compound	$\mathbf{Tl^{+}-O^{2-}}$ (Å) (Experiment)	$\mathbf{Tl^{+}-O^{2-}}$ (Å) (Calculated)
α-$Tl_2Te_2O_5$ [37]	Tl(1)-O: 2.580/2.584/2.646/2.840	Tl(1)-O: 2.513/2.377/2.722/2.844
	Tl(2)-O: 2.681/2.775/2.799/2.813	Tl(2)-O: 2.564/2.600/3.164/2.509
$Tl_2Te_3O_7$ [38]	Tl(1)-O: 2.471/2.588/2.700/2.828	Tl(1)-O: 2.465/2.561/2.560/2.663
	Tl(2)-O: 2.488/2.652/2.736/2.942	Tl(2)-O: 2.400/2.585/2.722/2.895
Tl_2TeO_3 [39]	Tl(1)-O: 2.548/2.746/2.810	Tl(1)-O: 2.728/2.577/2.679
	Tl(2)-O: 2.508/2.636/2.663/2.870	Tl(2)-O: 2.538/2.651/2.368/3.086

Table 3. $Tl^{+}-O^{2-}$ bond distances for three different Tl−Te−O crystalline structures based on experimental data and calculations from our IAP.

experimental density might lead to spurious effects due to the residual pressure in the cell, we extend the MD at 300 K in the NPT (constant number of particles, pressure and temperature) ensemble during a period of about 100ps. During this run we allow the cell volume to vary isotropically.

We note that polarisiblity effects are included in our simulation through core-shell IAP model. In particular, we resort to the DL_POLY Relaxed Shell Model (RSM) [51] implementation in which shells are massless and their motion follows the motion of the cores under the constraint of keeping vanishing forces acting on the shells.

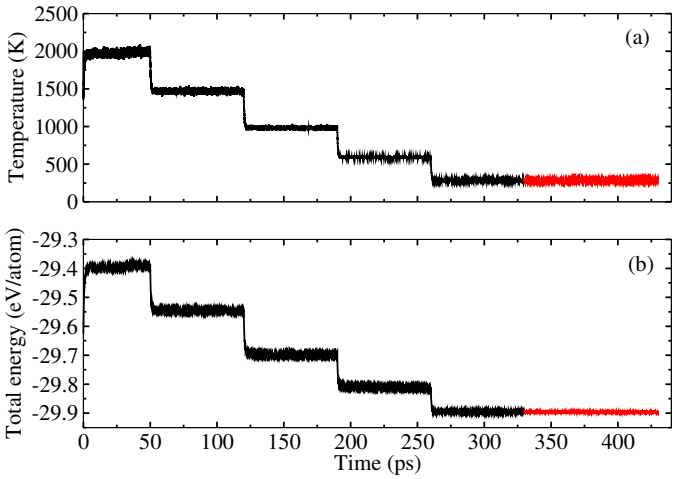

Figure 4. (a) Temperature and (b) Total Energy variation as function of Time for x=0.4 in $(TlO_{0.5})_x - (TeO_2)_{1-x}$; Black and Red lines represent NVT and NPT ensembles respectively.

The stability of our IAP is assessed during the MD run by looking at the total energy of the system. Fig. 4(b) shows the time-evolution of the total energy for $(TlO_{0.5})_x - (TeO_2)_{1-x}$ with x=0.4. At high temperatures, it is particularly difficult to account for core-shell models as shells move away from the cores due to their high kinetic energy resulting in simulation crash [30]. It is noteworthy that in our work the energy is conserved even for temperature as high as 2000K and during extended time-scales, reflecting the numerical accuracy of our IAP potential. This remains true as well for the NPT run where the cell size is allowed to vary. In this case, the stability of the potential is further proved by the very good stability of the dynamical variable, such as the lattice constant and the pressure for x=0.4, as shown in Fig. 5.

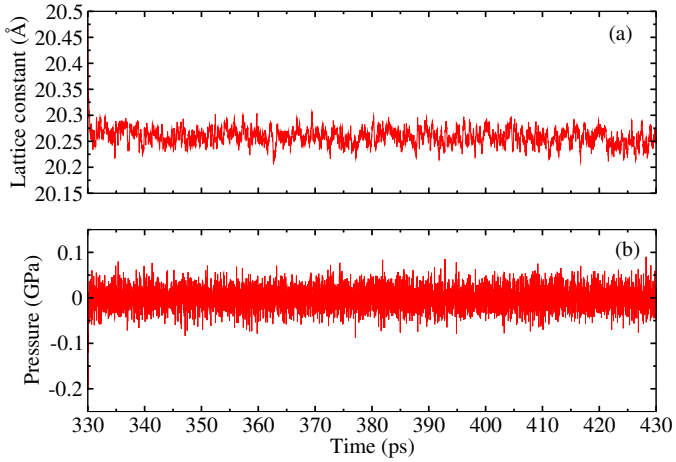

Figure 5. (a) Lattice constant of the smallest cell vector and (b) Pressure variation as a function of Time during NPT ensemble run.

We find that the pressure is very well conserved within a standard deviation of 0.016 GPa. The same behaviour is observed for the evolution of the lattice constant, where we find a standard deviation of 0.023 Å. For all the studied $(TlO_{0.5})_x - (TeO_2)_{1-x}$ models, we report the final equilibrium densities obtained by averaging the cell volume over the last 20ps during the NPT run. These values are also compared to experimental results from Ref. [40]. We find that our models successfully reproduce the experimental densities within an error of 3.02%, see table 4.

After checking the numerical stability and convergence of our IAP, we now confront the obtained atomic-scale models to experiments. In particular, we concentrate on measurable structural properties, the pair distribution function (PDF), and the static structure factor, in order to quantify the effectiveness of our IAP. The reduced X-ray PDFs $G(r)$ calculated using RINGS code [52] are presented in Fig. 6 and compared to their experimental counterpart from Ref. [40].

Overall, our models reproduce with a good accuracy the experimental pair distribution functions. In particular, the positions of the peaks located at 1.9 Å, 3.8 Å and 7.1 Å are in very good agreement with the experimental measurements. Furthermore, we find that the intensities of the peaks corresponding to Te−O distances ($\approx$ 1.9 Å) and Tl−O distances ($\approx$ 2.4 Å)

Concentration (x)	No. of Tl/Te/O (Total)	Experimental ρ (g.cm^{-3}) [40]	Calc. ρ (g.cm^{-3})	Lattice Constant (Å)	$\Delta\rho$ (%)
0.1	64/576/1184 (1824)	5.85	5.80	39.25/39.25/19.62	0.85
0.2	128/512/1088 (1728)	6.12	6.06	39.08/39.08/19.54	0.98
0.3	192/448/992 (1632)	6.40	6.30	38.98/38.98/19.49	1.56
0.4	288/432/1008 (1728)	6.68	6.50	40.51/40.51/20.25	2.69
0.5	360/360/900 (1620)	6.95	6.74	40.41/40.41/20.21	3.02

Table 4. Description of $(TlO_{0.5})_x - (TeO_2)_{1-x}$ amorphous system with various concentrations (x). Percentage change in density ($\Delta\rho$) between experimental (Expt.) density and after NPT run i.e. final calculated (Calc.) density. All configurations feature tetragonal simulation cell.

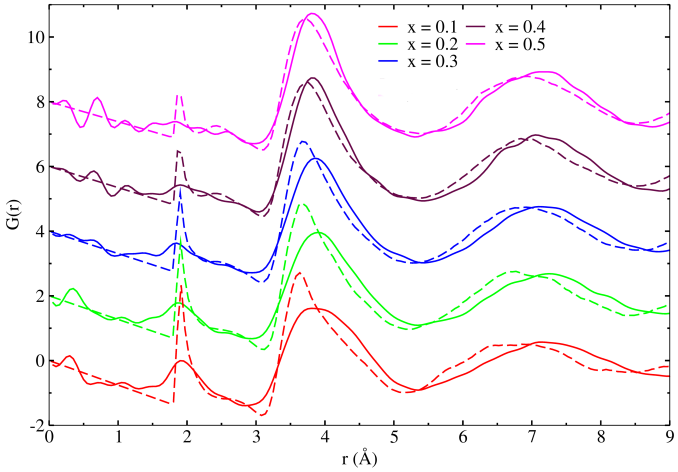

Figure 6. Comparison of G(r) between experiments and classical MD for $(TlO_{0.5})_x - (TeO_2)_{1-x}$ amorphous system with various concentrations (x). Solid lines: experimental; dashed lines: classical MD (analysed over the last 20ps of NPT run). A shift of 2 units is given to various concentrations for better analysis of the graph.

follow closely the trends observed experimentally. Specifically, our model reproduces the experimentally observed reduction of the intensity of the peak at ≈ 1.9 Å with increasing concentration of $TlO_{0.5}$ in TeO_2-based glass. In addition, the accuracy in reproducing the broad peak centered around 3.8 Å, which corresponds to Te−Te, Te−Tl and Tl−Tl distances, increases with higher concentration of $TlO_{0.5}$ modifier oxide. For r > 5 Å, we remark that, while the PDFs obtained from our models reproduce well the intensity of the broad peak in this region, they underestimate its position by about 0.5 Å. In addition, a better description of this peak might require a more sophisticated description of the Van der Waals interactions in the system. Nevertheless, we note that the integral of the peaks which directly correlate with the number of neighbors is very similar from theory and experiments.

The static structure factor S(q) is obtained from Fourier transforming the G(r) as follows:

$$S(q) = 1 + \int_0^{r_{max}} G(r)\frac{\sin(qr)}{q}dr \qquad (5)$$

where q and r_{max} are the scattering vector and upper limit of integration in real space, respectively. A comparison of experimental [40] and calculated S(q) is presented in figure 7. The first diffraction peak (FDP) centered around 2 Å^{-1} is fairly reproduced by our models in comparison to their experimental counterparts. It is also worth mentioning that similar to experiments our IAP records the increase of the amplitude of the FDP as a function of the concentration x of $(TlO_{0.5})_x - (TeO_2)_{1-x}$. Furthermore, similar to the behaviour observed for the G(r), the computed FDP tends to show a better reproduction of the experimental S(q) as the concentration of $TlO_{0.5}$ in the glass increases. Finally, we remark that for q vectors larger than 3 Å^{-1} our models remarkably reproduce the experimental pattern.

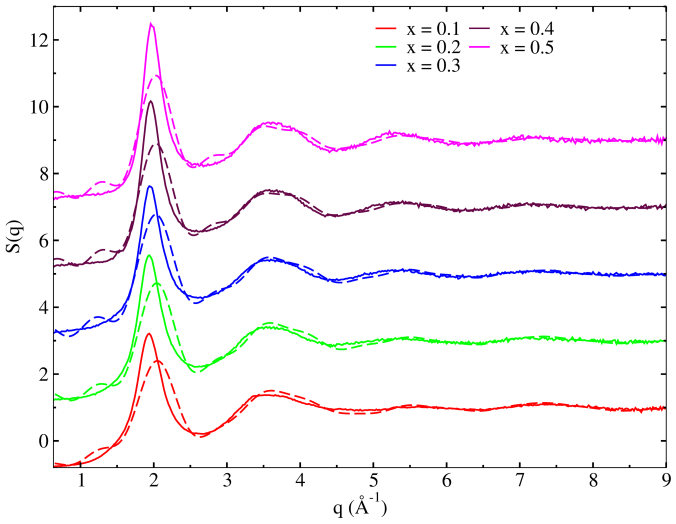

Figure 7. Comparison of S(q) X-ray diffraction between experiments and classical MD for $(TlO_{0.5})_x - (TeO_2)_{1-x}$ amorphous system with various concentrations (x). Solid lines: experimental; dashed lines: classical MD (analysed over the last 20ps of NPT run). A shift of 2 units is given to various concentrations for better analysis of the graph.

4. Conclusion

In summary, we obtained the Buckingham IAP parameters of Tl^+-O^{2-} and Tl^+-Tl^+ interaction through fitting experimental observables of α-$Tl_2Te_2O_5$, $Tl_2Te_3O_7$ and Tl_2TeO_3 crystalline compounds. The obtained potential has been tested on several other thallium (I) oxide based crystalline compounds and shows good accuracy in reproducing their atomic environments and lattice parameters with less than 6% of error. Furthermore, our potential is used to produce various $(TlO_{0.5})_x - (TeO_2)_{1-x}$ amorphous models ($0.1 \leq x \leq 0.5$) with less than 4% error on their final densities compared to reference experimental data. The obtained models feature good real and reciprocal space properties, in comparison to their experimental counterparts. The main peak positions and

intensities of the G(r) and S(q) are well reproduced, thus our IAP is able to reproduce the general features of the structures of $(TlO_{0.5})_x - (TeO_2)_{1-x}$ glasses. This work opens the way towards a inexpensive and accurate enough modelling of thallium (I) oxide based disordered systems.

5. Acknowledgments

This work was supported by the ANR via the TRAFIC project (ANR-18-CE08-0016-01) and F2MH project AAP NA 2019-1R1M01. Calculations were performed by using resources from GENCI (Grand Equipement National de Calcul Intensif) (Grants No. A0080910832). We used computational resources provided by the computing facilities MCIA (Mésocentre de Calcul Intensif Aquitain) of the Université de Bordeaux and of the Université de Pau et des Pays l'Adour.

Data availability statement

The raw/processed data required to reproduce these findings cannot be shared at this time due to technical or time limitations and will be made available before the publication of the paper online.

References

[1] G. D. Khattak, M. A. Salim, X-ray photoelectron spectroscopic studies of zinc–tellurite glasses, Journal of Electron Spectroscopy and Related Phenomena 123 (1) (2002) 47–55. doi:https://doi.org/10.1016/S0368-2048(01)00371-1.

[2] R. A. H. El-Mallawany, Tellurite Glasses Handbook : Physical Properties and Data, Second Edition, CRC Press, 2016. doi:10.1201/b11295.

[3] Elliott S., Medium-range structural order in covalent amorphous solids, Nature 354, 445–452 (1991). doi.org/10.1038/354445a0.

[4] Islam, M. S. and Winch, L. J., Defect chemistry and oxygen diffusion in the $HgBa_2$ $Ca_2Cu_3O_{8+\delta}$ superconductor: A computer simulation study, Phys. Rev. B 52, 10510-10515 (1995). 10.1103/PhysRevB.52.10510.

[5] Gale, Julian D. and Henson, Neil J., Derivation of interatomic potentials for microporous aluminophosphates from the structure and properties of berlinite, J. Chem. Soc., Faraday Trans. 90, 3175-3179 (1994). 10.1039/FT9949003175.

[6] Bush, Timothy S. and Gale, Julian D. and Catlow, C. Richard A. and Battle, Peter D., Self-consistent interatomic potentials for the simulation of binary and ternary oxides, J. Mater. Chem. 4, 831-837 (1994). 10.1039/JM9940400831.

[7] Jackson, R. A. and Catlow, C. R. A., Computer Simulation Studies of Zeolite Structure, Molecular Simulation 1, 207-224 (1988). 10.1080/08927028808080944.

[8] Lewis, G.V. and Catlow, C. R. A., Potential models for ionic oxides, J. Phys. C: Solid State Phys. 18, 1149 (1985). doi.org/10.1016/0038-1098(94)90351-4

[9] Binks D.J. and Grimes R. W., The non-stoichiometry of zincand chromium excess zinc chromite, Solid State Commun. 89, 921-4 (1994). doi.org/10.1088/0022-3719/18/6/010.

[10] D. Linda, J.-R. Duclère, T. Hayakawa, M. Dutreilh-Colas, T. Cardinal, A. Mirgorodsky, A. Kabadou, P. Thomas, Optical properties of tellurite glasses elaborated within the TeO_2–Tl_2O–Ag_2O and TeO_2–ZnO–Ag_2O ternary systems, Journal of Alloys and Compounds 561 (2013) 151–160. doi:https://doi.org/10.1016/j.jallcom.2013.01.172.

[11] Z. A. S. Mahraz, M. R. Sahar, S. K. Ghoshal, M. R. Dousti, Concentration dependent luminescence quenching of Er^{3+}-doped zinc boro-tellurite glass, Journal of Luminescence 144 (2013) 139–145. doi:https://doi.org/10.1016/j.jlumin.2013.06.050.

[12] N. Elkhoshkhany, S. Y. Marzouk, S. Shahin, Synthesis and optical properties of new fluoro-tellurite glass within (TeO_2-ZnO-LiF-Nb_2O_5-NaF) system, Journal of Non-Crystalline Solids 472 (2017) 39–45. doi:https://doi.org/10.1016/j.jnoncrysol.2017.07.012.

[13] S.-H. Kim, T. Yoko, S. Sakka, Linear and Nonlinear Optical Properties of TeO_2 Glass, Journal of the American Ceramic Society 76 (10) (1993) 2486–2490. doi:https://doi.org/10.1111/j.1151-2916.1993.tb03970.x.

[14] V. Dimitrov, T. Komatsu, Electronic polarizability, optical basicity and non-linear optical properties of oxide glasses, Journal of Non-Crystalline Solids 249 (2) (1999) 160–179. doi:https://doi.org/10.1016/S0022-3093(99)00317-8.

[15] H. Nasu, O. Matsushita, K. Kamiya, H. Kobayashi, K. Kubodera, Third harmonic generation from Li_2O-TiO_2-TeO_2 glasses, Journal of Non-Crystalline Solids 124 (2) (1990) 275–277. doi:https://doi.org/10.1016/0022-3093(90)90274-P.

[16] P. Naresh, Influence of TeO_2 on the UV, electrical and structural studies of Li_2O–ZnO– B_2O_3 glasses, Journal of Molecular Structure 1213 (2020) 128184. doi:https://doi.org/10.1016/j.molstruc.2020.128184.

[17] G. W. Brady, Structure of Tellurium Oxide Glass, The Journal of Chemical Physics 27 (1) (1957) 300–303. arXiv:https://doi.org/10.1063/1.1743690, doi:10.1063/1.1743690.

[18] Garaga, Mounesha N. and Werner-Zwanziger, U. and Zwanziger, J. W. and DeCeanne, A. and Hauke, B. and Bozer, K. and Feller, S., Short-Range Structure of TeO_2 Glass, The Journal of Physical Chemistry C 121 (50) (2017) 28117–28124. arXiv:https://doi.org/10.1021/acs.jpcc.7b08978, doi:10.1021/acs.jpcc.7b08978.

[19] L. S. El-Deen, M. A. Salhi, M. M. Elkholy, IR and UV spectral studies for rare earths-doped tellurite glasses, Journal of Alloys and Compounds 465 (1) (2008) 333–339. doi:https://doi.org/10.1016/j.jallcom.2007.10.104.

[20] N. Elkhoshkhany, R. Essam, E. S. Yousef, Influence of La_2O_3 on the structural, optical and thermal properties of TeO_2–ZnO–Li_2O–Nb_2O_5 glass, Journal of Non-Crystalline Solids 536 (2020) 119994. doi:https://doi.org/10.1016/j.jnoncrysol.2020.119994.

[21] K. M. Kaky, G. Lakshminarayana, S. Baki, I. Kityk, Y. Taufiq-Yap, M. Mahdi, Structural, thermal and optical absorption features of heavy metal oxides doped tellurite rich glasses, Results in Physics 7 (2017) 166–174. doi:https://doi.org/10.1016/j.rinp.2016.12.013.

[22] N. Tagiara, D. Palles, E. Simandiras, V. Psycharis, A. Kyritsis, E. Kamitsos, Synthesis, thermal and structural properties of pure TeO_2 glass and zinc-tellurite glasses, Journal of Non-Crystalline Solids 457 (2017) 116–125. doi:https://doi.org/10.1016/j.jnoncrysol.2016.11.033.

[23] M. Soulis, A. Mirgorodsky, T. Merle-Méjean, O. Masson, P. Thomas, M. Udovic, The role of modifier's cation valence in structural properties of TeO_2-based glasses, Journal of Non-Crystalline Solids 354 (2) (2008) 143–149, physics of Non-Crystalline Solids 11. doi:https://doi.org/10.1016/j.jnoncrysol.2007.07.032.

[24] Y. S. Rammah, M. S. Al-Buriahi, F. I. El-Agawany, Y. M. AbouDeif, E. S. Yousef, Investigation of mechanical features and gamma-ray shielding efficiency of ternary TeO_2-based glass systems containing Li_2O, Na_2O, K_2O, or ZnO, Ceramics International 46 (17) (2020) 27561–27569. doi:10.1016/j.ceramint.2020.07.248.

[25] B. Jeansannetas, S. Blanchandin, P. Thomas, P. Marchet, J. C. Champarnaud-Mesjard, T. Merle-Méjean, B. Frit, V. Nazabal, E. Fargin, G. Le Flem, M. O. Martin, B. Bousquet, L. Canioni, S. Le Boiteux, P. Segonds, L. Sarger, Glass Structure and Optical Nonlinearities in Thallium(I) Tellurium(IV) Oxide Glasses, Journal of Solid State Chemistry 146 (2) (1999) 329–335. doi:10.1006/jssc.1999.8355.

[26] M. Dutreilh-Colas, P. Thomas, J. Champarnaud-Mesjard, E. Fargin, New TeO_2 based glasses for nonlinear optical applications: study of the Tl_2O-TeO_2-Bi_2O_3, Tl_2O-TeO_2-PbO and Tl_2O-TeO_2-Ga_2O_3 systems, Physics and Chemistry of Glasses 44 (5) (2003) 349–352.

[27] T. Sekiya, N. Mochida, A. Ohtsuka, M. Tonokawa, Raman spectra of $MO_{1/2}$-TeO_2 (M = Li, Na, K, Rb, Cs and Tl) glasses, Journal of Non-Crystalline Solids 144 (1992) 128–144. doi:10.1016/S0022-3093(05)80393-X.

[28] O. Noguera, T. Merle-Méjean, A. Mirgorodsky, P. Thomas, J.-C. Champarnaud-Mesjard, Dynamics and crystal chemistry of tellurites. II. Composition- and temperature-dependence of the Raman spectra of x(Tl_2O)+(1-x)TeO_2 glasses: evidence for a phase separation?,

Journal of Physics and Chemistry of Solids 65 (5) (2004) 981–993. doi:https://doi.org/10.1016/j.jpcs.2003.11.020.

[29] M. Udovic, P. Thomas, A. Mirgorodsky, O. Masson, T. Merle-Mejean, C. Lasbrugnas, J. C. Champarnaud-Mesjard, T. Hayakawa, Formation domain and characterization of new glasses within the Tl_2O–TiO_2–TeO_2 system, Materials Research Bulletin 44 (2) (2009) 248–253. doi:10.1016/j.materresbull.2008.10.001.

[30] A. Gulenko, O. Masson, A. Berghout, D. Hamani, P. Thomas, Atomistic simulations of TeO_2 -based glasses: interatomic potentials and molecular dynamics, Phys. Chem. Chem. Phys. 16 (27) (2014) 14150–14160. doi:10.1039/C4CP01273A.

[31] L. Torzuoli, A. Bouzid, P. Thomas, O. Masson, An enhanced core–shell interatomic potential for Te–O based oxides, Materials Research Express 7 (1) (2020) 015202. doi:10.1088/2053-1591/ab6128.

[32] B. W. H. van Beest, G. J. Kramer, R. A. van Santen, Force fields for silicas and aluminophosphates based on ab-initio calculations, Phys. Rev. Lett. 64 (1990) 1955–1958. doi:10.1103/PhysRevLett.64.1955.

[33] X.-Y. Qu, X.-F. Gou, T.-G. Wang, A highly accurate interatomic potential for $LaMnO_3$ perovskites with temperature-dependence of structure and thermal properties, Computational Materials Science 193 (2021) 110406. doi:https://doi.org/10.1016/j.commatsci.2021.110406.

[34] P. P. Ewald, Die Berechnung optischer und elektrostatischer Gitterpotentiale, Annalen der Physik 369 (3) (1921) 253–287. arXiv:https://onlinelibrary.wiley.com/doi/pdf/10.1002/andp.19213690304, doi:https://doi.org/10.1002/andp.19213690304.

[35] B. G. Dick, A. W. Overhauser, Theory of the Dielectric Constants of Alkali Halide Crystals, Phys. Rev. 112 (1958) 90–103. doi:10.1103/PhysRev.112.90.

[36] J. D. Gale, A. L. Rohl, The General Utility Lattice Program (GULP), Molecular Simulation 29 (5) (2003) 291–341. arXiv:https://doi.org/10.1080/0892702031000104887, doi:10.1080/0892702031000104887.

[37] B. Jeansannetas, P. Thomas, J. Champarnaud-Mesjard, B. Frit, Crystal structure of α-$Tl_2Te_2O_5$, Materials Research Bulletin 33 (11) (1998) 1709–1716. doi:https://doi.org/10.1016/S0025-5408(98)00171-8.

[38] B. Jeansannetas, P. Thomas, J. Champarnaud-Mesjard, B. Frit, Crystal structure of $Tl_2Te_3O_7$, Materials Research Bulletin 32 (1) (1997) 51–58. doi:https://doi.org/10.1016/S0025-5408(96)00160-2.

[39] B. Frit, D. Mercurio, P. Thomas, J.-C. Champarnaud-Mesjard, Refinement of the crystal structure of dithallium(I) trioxotellurate(IV), TI_2TeO_3, Zeitschrift für Kristallographie - New Crystal Structures 214 (4) (1999) 439–440. doi:doi:10.1515/ncrs-1999-0419.

[40] Torzuoli, Lyna, Etude de la structure des verres des systèmes TeO_2-M_xO_y (M = Ti, TI) par diffusion totale des rayons X et dynamique moléculaire, Ph.D. thesis, Universite de Limoges (2020).

[41] S. M. Woodley, P. D. Battle, J. D. Gale, C. Richard A. Catlow, The prediction of inorganic crystal structures using a genetic algorithm and energy minimisation, Phys. Chem. Chem. Phys. 1 (1999) 2535–2542. doi:10.1039/A901227C.

[42] J. E. Saal, S. Kirklin, M. Aykol, B. Meredig, C. Wolverton, Materials Design and Discovery with High-Throughput Density Functional Theory: The Open Quantum Materials Database (OQMD), JOM 65 (11) (2013) 1501–1509. doi:10.1007/s11837-013-0755-4.

[43] S. Kirklin, J. E. Saal, B. Meredig, A. Thompson, J. W. Doak, M. Aykol, S. Rühl, C. Wolverton, The Open Quantum Materials Database (OQMD): assessing the accuracy of DFT formation energies, npj Computational Materials 1 (1) (2015) 1–15, number: 1 Publisher: Nature Publishing Group. doi:10.1038/npjcompumats.2015.10.

[44] C. G. Broyden, The Convergence of a Class of Double-rank Minimization Algorithms 1. General Considerations, IMA Journal of Applied Mathematics 6 (1) (1970) 76–90. arXiv:https://academic.oup.com/imamat/article-pdf/6/1/76/2233756/6-1-76.pdf, doi:10.1093/imamat/6.1.76.

[45] R. Fletcher, A new approach to variable metric algorithms, The Computer Journal 13 (3) (1970) 317–322. arXiv:https://academic.oup.com/comjnl/article-pdf/13/3/317/988678/130317.pdf, doi:10.1093/comjnl/13.3.317.

[46] D. Goldfarb, A family of variable-metric methods derived by variational means, Mathematics of Computation 24 (109) (1970) 23–26. doi:10.1090/S0025-5718-1970-0258249-6.

[47] D. F. Shanno, Conditioning of quasi-Newton methods for function minimization, Mathematics of Computation 24 (111) (1970) 647–656. doi:10.1090/S0025-5718-1970-0274029-X.

[48] P. Nicolini, T. Polcar, A comparison of empirical potentials for sliding simulations of MoS2, Computational Materials Science 115 (2016) 158–169. doi:https://doi.org/10.1016/j.commatsci.2016.01.013.
URL `https://www.sciencedirect.com/science/article/pii/S0927025616000197`

[49] L. Martínez, R. Andrade, E. G. Birgin, J. M. Martínez, PACKMOL: A package for building initial configurations for molecular dynamics simulations, Journal of Computational Chemistry 30 (13) (2009) 2157–2164. arXiv:https://onlinelibrary.wiley.com/doi/pdf/10.1002/jcc.21224, doi:https://doi.org/10.1002/jcc.21224.

[50] I. T. Todorov, W. Smith, K. Trachenko, M. T. Dove, DL_POLY_3: new dimensions in molecular dynamics simulations via massive parallelism, J. Mater. Chem. 16 (20) (2006) 1911–1918, publisher: The Royal Society of Chemistry. doi:10.1039/B517931A.

[51] P. J. D. Lindan, M. J. Gillan, Shell-model molecular dynamics simulation of superionic conduction in CaF_2, Journal of Physics: Condensed Matter 5 (8) (1993) 1019–1030. doi:10.1088/0953-8984/5/8/005.

[52] S. L. Roux, P. Jund, Ring statistics analysis of topological networks: New approach and application to amorphous GeS_2 and SiO_2 systems, Computational Materials Science 49 (1) (2010) 70–83. doi.org/10.1016/j.commatsci.2010.04.023.

[53] Database of Published Interatomic Potential Parameters, `https://www.ucl.ac.uk/klmc/Potentials/`.